AIP | Journal of Applied Physics

Model of native point defect equilibrium in Cu2ZnSnS4 and application to one-zone annealing

V. Kosyak, N. B. Mortazavi Amiri, A. V. Postnikov, and M. A. Scarpulla

Citation: J. Appl. Phys. **114**, 124501 (2013); doi: 10.1063/1.4819206
View online: http://dx.doi.org/10.1063/1.4819206
View Table of Contents: http://jap.aip.org/resource/1/JAPIAU/v114/i12
Published by the AIP Publishing LLC.

Model of native point defect equilibrium in Cu_2ZnSnS_4 and application to one-zone annealing

V. Kosyak,[1,2,a)] N. B. Mortazavi Amiri,[3] A. V. Postnikov,[3] and M. A. Scarpulla[1,4]
[1]*Materials Science and Engineering, University of Utah, Salt Lake City, Utah 84112, USA*
[2]*Department of Electronics and Computer Technology, Sumy State University, Sumy UA-40007, Ukraine*
[3]*Institut Jean Barriol, Lorraine University, Metz F-57078, France*
[4]*Electrical and Computer Engineering, University of Utah, Salt Lake City, Utah 84112, USA*

(Received 13 April 2013; accepted 8 August 2013; published online 23 September 2013)

We report a quasichemical model for point defect equilibrium in Cu_2ZnSnS_4 (CZTS). An *ab initio* calculation was used to estimate the changes in the phonon spectrum of CZTS due to trial point defects and further vibrational free energy, which in turn influences the final defect concentrations. We identify the dominant point defects and estimate the free carrier concentrations as functions of the Zn, Cu, and Sn chemical potentials, the sulfur chemical potential being set by the vapor-solid equilibrium with elemental S at the same temperature as the sample (one-zone annealing). As hinted by calculated low formation enthalpies, either the Cu vacancy (V_{Cu}^{-}) or Cu on Zn antisite (Cu_{Zn}^{-}) acceptors are expected to dominate over a wide range of cation chemical potentials. However, the sulfur vacancy (V_S^{2+}) becomes a dominant compensating donor especially for one-zone annealing conditions. We also find that different native defects induce distinct perturbations to the vibrational free energy, resulting in non-trivial qualitative and quantitative shifts in the defect equilibrium. At typical annealing temperatures and Zn-rich conditions, this may introduce especially strong modulations in the concentrations of Zn_{Sn}^{2-} and, contrary to enthalpic predictions, of Zn_{Cu}^{+} compensating donors. The modeling indicates that one-zone processing should result in CZTS, which is p-type but extremely compensated because native donor defects are stabilized by the low Fermi level and finite-temperature effects.
 [http://dx.doi.org/10.1063/1.4819206]

I. INTRODUCTION

$Cu_2ZnSn(S,Se)_4$ (CZTSSe) is an alloy system promising for use as thin film solar cell absorber layer at terawatt scale.[1,2] Beyond the fact that CZTSSe has the requisite high optical absorption coefficient and direct band gap matched to the solar spectrum, all of its constituent elements are abundant both geologically and industrially.[1,3,4] The maximal efficiencies of solar cells based on the pure sulfide CZTS and on the mixed sulfoselenide $Cu_2ZnSn(S,Se)_4$ are 8.4% and 11.1%, respectively.[5,6] CZTS is especially interesting because of its potential for high open circuit voltage (V_{OC}). However, the production of high-performance CZTS thin films is hindered by competition with at least 8 secondary phases;[7,8] moreover, this material is known to exist in three ordered polymorphs as well as disordered structures;[9,10] it is typically prepared as polycrystalline films,[11,12] and routinely contains large concentrations of native defects.[13–16] In heterojunction thin film solar cells, the charged point imperfections in the lower-doped absorber layer control the depletion width and dominate defect-mediated recombination within it.[17,18] Thus, the prediction of point defect concentrations is extremely important and can lead to insights which can help to identify processing routes for absorber layers resulting in high solar cell performance.

In the canonical work by Kröger, the theoretical analysis of point defects in ceramics and semiconductors is based on quasichemical theory.[19] This approach allows to calculate the concentrations of isolated point defects in an otherwise perfect crystal for various thermodynamic boundary conditions.[19–23] In well-studied materials having a limited number of enthalpically probable defects, reaction constants are determined by the fitting of a dominant charged defect's concentration to the measured free carrier density.[19,20,23] Therefore, many quasichemical models are based on experimental results applicable over a small range of single-crystal annealing conditions. In the general case where multiple defects may have comparable concentrations, the fitting of models to experiment can be ambiguous.

Typically, calculations of point defect equilibrium are performed assuming conditions of thermodynamic equilibrium between a crystal and a gas phase at a high processing temperature. On the other hand, most characterization experiments on thin film samples are carried out at, or below, the room temperature.[19,22] Calculations of full equilibrium at room temperature correspond to cooling infinitely slowly. In calculations that simulate quenching, the total concentrations of point defects (both neutral and charged ones, for each type of defect) are computed at the processing temperature, after which the carrier statistics is recalculated at room temperature.[19,20,23,24] If applied correctly, such quasichemical models are capable of encompassing the full range of temperature-time annealing profiles and even variations in the chemical potentials during processing.

The development of computational techniques and computing power has progressed sufficiently to allow reasonably

a)Electronic mail: vvkosyak@gmail.com

accurate prediction of formation and ionization energies of point defects from first principles.[20,22–30] The use of these values in quasichemical modeling has been shown to provide sufficient correlation between experimental and calculated results such that useful insight can be gained.[20,22–24] Predicted defect concentrations are exponentially sensitive to the calculated formation energies; therefore, it is still necessary to defer to experimental results.[23] However, in the current early stage of study of CTZSSe, theoretical results are the only ones available which can identify specific defects and their properties. We thus seek in this work to extract trends and insights which can guide experiment and help to explain observed phenomena, rather than make exact numerical predictions. In the best quasichemical analyses of point defects in semiconductors, large single crystals are studied.[19,23] In the case of thin film samples, free surfaces and grain boundaries may modify the defect equilibrium making the modeling of defect populations more complicated.[31–33] Deviations from quasichemical model predictions, especially in polycrystalline thin film samples containing extended structural defects, should be anticipated.

The usual quasichemical formalism assumes a dilute arrangement of non-interacting defects. This means first that they are sufficiently widely spaced such that formation energies and discrete charge transition levels are not modified by interactions between defects, in the sense that neither are the corresponding levels shifted, nor corresponding energy-resolved distributions broadened. Second, it means that the dilute approximations for the configurational entropy used to derive the Boltzmann statistical occupations of defects on (sub)lattice sites are not violated. These translate into statements that the total defect concentration should neither result in orbital overlap amongst pairs of defects nor exceed a small fraction of any sublattice's site density. A third principle results from the common use of non-degenerate carrier statistics for the valence and conduction bands. This is that the defect-related total density of states should be small compared to the bands' effective densities of states. In numerical terms, these constraints suggest rule-of-thumb upper limits on the total defect density (sum of all defects) in the 10^{18}–$10^{20}\,\mathrm{cm}^{-3}$ for the model to remain self-consistent. Therefore, the modeling within parameter ranges resulting in predicted concentrations above this threshold should be treated with suspicion as the model's assumptions will be broken.

Many experimental[34–36] and theoretical[27,28,37] studies of point defects in multicompound semiconductors such as the I–III–VI_2 semiconductor Cu(In,Ga)Se_2 reveal a complicated interplay of point defects and their complexes. Likely dominant defects in $CuInSe_2$ and Cu(In,Ga)Se_2 are the vacancy of copper V_{Cu}, III on I antisite $In(Ga)_{Cu}$, I on III antisite $Cu_{In(Ga)}$, and complexes of these defects such as $\left(2V_{Cu} + In(Ga)_{Cu}\right)$.[27,37,38] Later, it was proposed that chalcogen vacancies V_{Se} (Ref. 28) and divacancy complexes $V_{Se} - V_{Cu}$ (Refs. 35, 39, and 40) have strong effects on the properties of chalcopyrite thin films. Most of the theoretical studies are focused on first-principles calculation of point defect formation energies, whereas only a few papers[41,42] attempted to make numerical predictions based on quasichemical models.

A number of papers dealing with first-principles calculation of the point defect formation energies (ΔE or ΔU, defined in Appendix A) for CZTS were published recently.[13–16] These may be taken as formation enthalpies ΔH assuming that the change in the pressure-volume product is insignificant. From these results, we extracted the "self-enthalpies" of formation which are independent of the chemical potentials, in order to be able to compute formation enthalpies for any arbitrary set of imposed chemical potentials. From these self-enthalpies, the copper and zinc vacancies (V_{Cu}, V_{Zn}) and copper-on-zinc and copper-on-tin antisites (Cu_{Zn}, Zn_{Sn}) should be the dominant acceptor-like defects for a wide range of chemical potential conditions.[13–16] The sulfur vacancy and zinc-on-copper antisite (V_S, Zn_{Cu}) should be the dominant donor-like native defects.[13–16] However, future work should include all possible native and extrinsic effects to account for small concentrations of defects we are not considering which may still act as effective recombination centers. Also, otherwise unfavorable compensating defects can be stabilized a very low or very high Fermi-levels especially as the band gap becomes larger.

Two problems appear if defect equilibrium for a multicompound semiconductor is computed directly, using only *ab initio* defect formation energies ΔU (in the standard thermodynamic nomenclature) and constraining the chemical potentials for the constituent elements by the computed formation energies of other phases in the phase diagram (as was done in Refs. 13–16). First, a total free energy of defect formation given by either Helmholtz $F \equiv U\text{-}TS$ or Gibbs potential $G \equiv F + pV$ (T being temperature, S entropy, P pressure, and V volume) must be used at finite temperatures to calculate the point defect equilibrium, while electronic structure calculations invoking the Born-Oppenheimer approximation are done by definition at 0 K. Thus, the specific heat should be integrated from 0 K to the temperature of interest to obtain the $-TS$ term. This is extremely important especially at annealing temperatures, where this entropic term may completely dominate the total free energy. For small carrier concentrations in semiconductors, the lattice specific heat dominates and the problem reduces to determining and integrating the phonon related free energy.

The second issue is primarily related to the fact that the change in free energy ΔF or ΔG for the formation of any phase is a function of temperature—explicitly because of the T in the TS product, but also implicitly because of the temperature dependences of the total specific heats of the reactants and products. Moreover, the free energy of formation of a phase at stoichiometry will differ from that with deviation from stoichiometry. For very small concentrations of defects, this can probably be neglected. However, for secondary phases such as $Cu_xS(Se)$, $Sn_xS(Se)$, and $Cu_xSn(S,Se)_y$, which are adjacent to CZTS (CZTSSe) in the quaternary phase diagram and themselves may have variable stoichiometry, this is not obvious *a priori*. Therefore, the extremal limits on the chemical potentials in the single phase region for CZTS(Se) calculated at the single phase-mixed phase boundaries at 0 K must be corrected for finite temperatures and self-consistently for departures from stoichiometry

of the neighboring phases, again using the specific heats of all phases considered. Since this is very involved and actually not possible at the time of writing because of lack of verified thermodynamic parameters, we will estimate reasonable ranges of the chemical potentials for single-phase CZTS herein.

It is obvious that the formation of point defects with sufficiently high density must perturb the phonon spectrum of a crystalline phase and, therefore, its free energy at any given temperature. The effects of vibrational free energy on quasichemical analysis of point defect formation have been considered in some works.[22,23,25] The *ab initio* study of vibrational properties of perfect CZTS(Se) crystal was started recently[43,44] and did in fact motivate the present work. Also, it is of great interest in CZTS(Se) to construct a general model for point defect densities, which may be useful to predict and understand samples' properties. This is especially true because experimental data[45–47] on point defects are currently sparse in the literature. Therefore, in this work we present a general model framework for computation of point defect equilibrium in CZTS thin film processing and begin to explore the influence of the changes in the phonon density of states (phDOS) brought about by point defect formation.

II. CALCULATION METHOD

A. Quasichemical model

As was mentioned above, first-principles calculations[13–16] determine the lowest-formation-energy native acceptor-like defects to be V_{Cu}, V_{Zn}, Cu_{Zn}, Zn_{Sn}, and as well as the lowest-formation-energy native donor-like defects—V_S and Zn_{Cu}.[13] Other native defects have significantly higher formation energies, so we focused on the six mentioned above.

Besides perfect CZTS, pure reference states were included for each component and described by the chemical potentials μ_{Cu}, μ_{Zn}, μ_{Sn}, and μ_S. In general, each chemical potential may be varied in experiments by supplying the elemental components in different forms, by keeping pure elemental sources at different temperatures, or by exciting internal degrees of freedom (e.g., by plasma ionization or non-ionizing excitation of electronic states). Clearly, the possible processing parameter space is immense. We thus first consider the simplest subset of commonly used annealing procedures in which a CZTS sample is held in a closed container with a supply of pure sulfur, whereby the entire system is held at the same temperature—i.e., "one-zone" annealing as shown in Fig. 1. We constrain the sulfur chemical potential to its value given by the experimental temperature-dependent S_2 vapor pressure as described in Appendix B.

Quasichemical theory commonly assumes the existence of thermodynamic equilibrium between the compound of interest and reference states (solid or gas phase) of the compound's components. For example, the formation of copper vacancies can be considered as transitions of copper atoms from a perfect crystal to the reference state, see Fig. 1, which may be described with the following equilibrium reaction:

$$Cu_2ZnSnS_4 \leftrightarrow CuV^0_{Cu}ZnSnS_4 + Cu_R, \tag{1}$$

in which Cu_2ZnSnS_4 is a perfect crystal, $CuV^0_{Cu}ZnSnS_4$ is a crystal with a copper vacancy, and Cu_R indicates a Cu atom in the reference state. In theoretical works on CZTS,[13–16] the pure elemental solid was considered as a reference state. However, at high temperature annealing conditions the vapor phase in equilibrium with the elemental crystal can also act as a reference state.[22–24,29,30] We arbitrarily vary the metal chemical potentials later in the calculations, which can be viewed as varying the partial pressure of the gas-phase references for each metal. In some analogy, it can be done in the process of thermal evaporation by changing the source temperatures. Boundaries on the chemical potentials corresponding to the transition from single-phase CZTS to two-phase regions must be determined later. While phase boundaries have been established in composition space at discrete temperatures,[48] the boundary chemical potentials are not currently available. Thus, the predictions of our model should only be literally interpreted for conditions resulting in small deviations in stoichiometry of the CZTS for which it is known that CZTS remains single phase. We seek to investigate trends in behavior, especially in how the high temperature effects we have included modify the predictions made at 0 K.

With respect to reaction (1), the balance of the total chemical potentials is given as

$$\mu^t_{Cu_2ZnSnS_4} - \mu^t_{CuV^0_{Cu}ZnSnS_4} - \mu^t_{Cu} = 0. \tag{2}$$

Here, $\mu^t_{Cu_2ZnSnS_4}$, $\mu^t_{CuV^0_{Cu}ZnSnS_4}$, and μ^t_{Cu} are the total chemical potentials of the perfect crystal, crystal containing a copper vacancy, and the copper atoms reservoir.

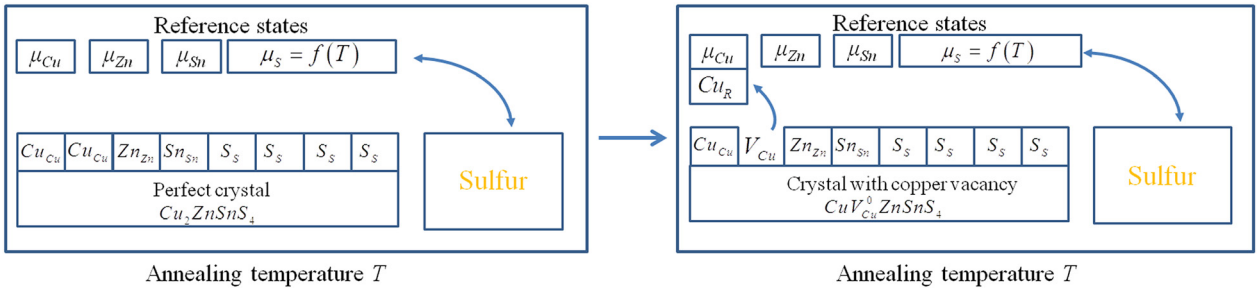

FIG. 1. Transition of the Cu atom from the CZTS primitive unit cell to the reference state and further formation of Cu vacancy with respect to Eq. (1).

The concentration of the neutral copper vacancies can be expressed from Eqs. (2) and (A19) within statistical thermodynamics[49] as

$$[V^0_{Cu}] = [Cu_{Cu}]\exp\left(-\frac{F^{vib}_{CuV^0_{Cu}ZnSnS_4} - F^{vib}_{Cu_2ZnSnS_4}}{k_bT}\right) \times \exp\left(-\frac{E^0_{Cu_2V^0_{Cu}ZnSnS_4} - E^0_{Cu_2ZnSnS_4} + \varepsilon^0_{Cu} + \mu_{Cu}}{k_bT}\right) g_{V^0_{Cu}}. \quad (3)$$

Here, $[Cu_{Cu}]$ is the total concentration of copper lattice sites in the CZTS crystal $= 1.248 \times 10^{22}\,\mathrm{cm}^{-3}$ (note that we do not differentiate the two crystallographically distinct Cu lattice sites in kesterite for this work), $F^{vib}_{CuV^0_{Cu}ZnSnS_4}$ and $F^{vib}_{Cu_2ZnSnS_4}$ are the vibrational free energies of the CZTS crystal with copper vacancies and perfect CZTS crystal (respectively), $E^0_{Cu_2V^0_{Cu}ZnSnS_4}$, $E^0_{Cu_2ZnSnS_4}$, and ε^0_{Cu} are the energies at $T = 0\,\mathrm{K}$ of perfect CZTS, CZTS with copper vacancies V^0_{Cu}, and the copper atoms in the gas phase, respectively, μ_{Cu} is the copper reference chemical potential, $g_{V^0_{Cu}}$ is the degeneracy of the neutral copper vacancy, k_b is the Boltzmann constant, and T is the annealing temperature.

Taking into account that the energy of point defect formation is the sum of energies $\Delta E_{V^0_{Cu}} = E^0_{Cu_2V^0_{Cu}ZnSnS_4} - E^0_{Cu_2ZnSnS_4} + \varepsilon^0_{Cu}$, and the difference in vibrational free energy between defected crystal and perfect crystal was denoted as $\Delta F^{vib}_{V^0_{Cu}} = F^{vib}_{CuV^0_{Cu}ZnSnS_4} - F^{vib}_{Cu_2ZnSnS_4}$ the concentration of copper vacancies can be expressed as the following equation:

$$[V^0_{Cu}] = [Cu_{Cu}]\exp\left(-\frac{\Delta F^{vib}_{V^0_{Cu}}}{k_bT}\right)\exp\left(-\frac{\Delta E_{V^0_{Cu}} + \mu_{Cu}}{k_bT}\right) g_{V^0_{Cu}}. \quad (4)$$

The concentrations of the other five neutral defects considered are similarly given by

$$[V^0_{Zn}] = [Zn_{Zn}]\exp\left(-\frac{\Delta F^{vib}_{V^0_{Zn}}}{k_bT}\right)\exp\left(-\frac{\Delta E_{V^0_{Zn}} + \mu_{Zn}}{k_bT}\right) g_{V^0_{Zn}}, \quad (5)$$

$$[Cu^0_{Zn}] = [Zn_{Zn}]\exp\left(-\frac{\Delta F^{vib}_{Cu^0_{Zn}}}{k_bT}\right) \times \exp\left(-\frac{\Delta E_{Cu^0_{Zn}} + \mu_{Zn} - \mu_{Cu}}{k_bT}\right) g_{Cu^0_{Zn}}, \quad (6)$$

$$[Zn^0_{Sn}] = [Sn_{Sn}]\exp\left(-\frac{\Delta F^{vib}_{Zn^0_{Sn}}}{k_bT}\right) \times \exp\left(-\frac{\Delta E_{Zn^0_{Sn}} + \mu_{Sn} - \mu_{Zn}}{k_bT}\right) g_{Zn^0_{Sn}}, \quad (7)$$

$$[Zn^0_{Cu}] = [Cu_{Cu}]\exp\left(-\frac{\Delta F^{vib}_{Zn^0_{Cu}}}{k_bT}\right) \times \exp\left(-\frac{\Delta E_{Zn^0_{Cu}} + \mu_{Cu} - \mu_{Zn}}{k_bT}\right) g_{Zn^0_{Cu}}, \quad (8)$$

$$[V^0_S] = [S_S]\exp\left(-\frac{\Delta F^{vib}_{V^0_S}}{k_bT}\right)\exp\left(-\frac{\Delta E_{V^0_S} + \mu_S}{k_bT}\right) g_{V^0_S}, \quad (9)$$

in which $[Zn_{Zn}]$, $[Sn_{Sn}]$, and $[S_S]$ are the total concentration of the zinc, tin, and sulfur lattice sites in a perfect kesterite CZTS crystal ($[Zn_{Zn}] = [Sn_{Sn}] = 6.239 \times 10^{21}\,\mathrm{cm}^{-3}$ and $[S_S] = 2.496 \times 10^{21}\,\mathrm{cm}^{-3}$).

In the case of the sulfur vacancy V^0_S, see Eq. (9), we have considered equilibrium between the CZTS crystal and S_2 diatomic sulfur gas with the total chemical potential μ_{S_2}, because both its reactivity and vapor pressure dominate those of the other equilibrium S vapor species (e.g., S_3, S_4, …, S_8).[50] The chemical potential may be computed from experimentally determined standard thermodynamic functions[30] or from statistical thermodynamics.[22,29] In the latter case, the total chemical potential of S_2 could be calculated through the total energy of the molecule[19,22,29,49,51,52] as Eq. (B2); the results of calculation are shown in Fig. 2. We then took the chemical potential of a single S atom, which participates in defect formation reactions as $\mu_S = 0.5\mu_{S_2}$.[29,30]

It should be noted that the derived expression for the defect formation energy $\Delta E_{V^0_{Cu}} = E^0_{Cu_2V^0_{Cu}ZnSnS_4} - E^0_{Cu_2ZnSnS_4} + \varepsilon^0_{Cu}$ in Eq. (4) corresponds to the form used in those *ab initio* works, which ignore the finite temperature vibrational energy.[9,13–16]

$$\Delta H_{D,q} = (E_{D,q} - E_{perfect}) + \sum_i n_i(E_i + \mu_i) + q(E_{VBM} + \mu_F), \quad (10)$$

in which $E_{D,q}$ is the total energy of the crystal with the defect in charge state q ($q = 0$ for neutral defects), $E_{perfect}$ is the energy of the perfect crystal, n_i is the number of i atoms transferred from the crystal to the reservoir ($n = +1$ in the

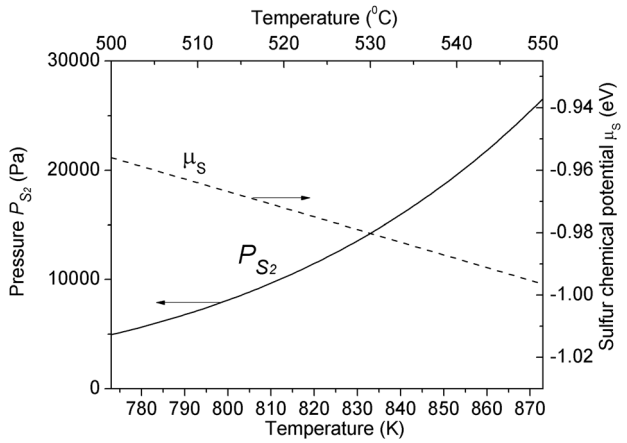

FIG. 2. Pressure of the diatomic sulfur P_{S_2} (solid line) and chemical potential of the monoatomic sulfur μ_S (dashed line) as a function of the annealing temperature.

TABLE I. Point defects formation parameters.

Type of the defect	Neutral defect formation energy ΔE (eV)[a]	Change in vibrational free energy ΔF^{vib} (eV) at $T = 550\,^{\circ}\mathrm{C}$	The transition energy level of the defects (eV) (valence band maximum = 0)[a]	Degeneracy factor
V_{Cu}	0.76	0.058	$\varepsilon_{V_{Cu}^{-}} = 0.02$	$g_{V_{Cu}^{0}} = 1$ $g_{V_{Cu}^{-}} = 2$
V_{Zn}	2.14	−0.084	$\varepsilon_{V_{Zn}^{2-}} = 0.22$	$g_{V_{Zn}^{0}} = 1$ $g_{V_{Zn}^{2-}} = 2$
Cu_{Zn}	1.04	−0.101	$\varepsilon_{Cu_{Zn}^{-}} = 0.12$	$g_{Cu_{Zn}^{0}} = 1$ $g_{Cu_{Zn}^{-}} = 2$
Zn_{Sn}	−0.04	0.029	$\varepsilon_{Zn_{Sn}^{2-}} = 0.23$	$g_{Zn_{Sn}^{0}} = 1$ $g_{Zn_{Sn}^{2-}} = 2$
V_S	1.71	−0.27	$\varepsilon_{V_S^{2+}} = 0.66$	$g_{V_S^{0}} = 1$ $g_{V_S^{2+}} = 0.5$
Zn_{Cu}	1.4	−0.42	$\varepsilon_{Zn_{Cu}^{+}} = 1.35$	$g_{Zn_{Cu}^{0}} = 1$ $g_{Zn_{Cu}^{+}} = 0.5$

[a]Reference 13.

cases of vacancy formation), E_i is the total energy of the reference state for each element, μ_i is the reference chemical potential, E_{VBM} is the valance band maximum, and μ_F is the electron chemical potential or Fermi energy.

In order to calculate how the concentrations of neutral point defects depend on chemical potential according to Eqs. (4)–(9), it is first necessary to determine the changes in vibrational free energy ΔF^{vib} and formation energy ΔE of point defects.

B. Formation energies

In Ref. 13, the total energy of neutral point defect formation was calculated at a set of discrete points in the chemical potential space according to Eq. (10). Because our purpose is to calculate point defect concentrations over a range of chemical potentials, we have extracted the values of ΔE from the total defect formation energies tabulated in Ref. 13 using $\Delta E = \Delta H_{D,q} - \sum_i n_i \mu_i$ and listed them in Table I. These bare formation energy differences show that some previously discounted defects may in fact have low formation enthalpies in certain chemical potential regimes (e.g., Zn_{Sn}).

C. Calculation of the vibrational free energy

First-principles calculations of the phDOS of 64-atom CZTS supercells containing different isolated point defects have been done by the SIESTA *ab initio* package[53–55] using the local density approximation (LDA). The details of calculation are as outlined in Ref. 44, with the substitution of Se by S in the present case. For the perfect CZTS and for each defect system, first an unconstrained lattice relaxation was carried out followed by calculation of the lattice vibrational spectrum in the "frozen phonon" approach. Each atom underwent a trial displacement by ±0.04 Bohr along the three Cartesian directions allowing the calculation, by finite differences, of the force constants including influences from all of the atoms. The diagonalization of the dynamic equations yielded $64 \times 3 = 192$ (or 189, in case of vacancy-containing supercells) vibration frequencies, corresponding to the zone-center modes of the supercell. This discrete spectrum included a considerable amount of off-zone-center modes of the underlying prototype (kesterite) unit cell, downfolded onto $k = 0$ of the supercell. We considered this a fair approximation of the "true" vibrational spectrum of the system containing defects. This approximation is acceptable because our primary interest is in the integration of the phDOS with a smoothly varying function (as described below) as opposed to the spectrum itself. The resulting densities of modes for the perfect supercell and the modifications induced by different point defects (broadened to half-width of $2\,\mathrm{cm}^{-1}$ for better visibility only) are shown in Fig. 3.

The Helmholtz free energy of a system of harmonic oscillators with a continuous density of modes versus frequency $g(\omega)$ is given by

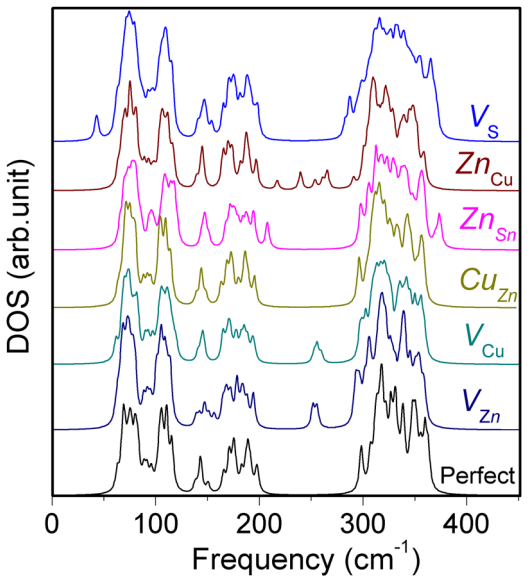

FIG. 3. Calculated phDOS of the perfect and defect-containing 64-atomic site CZTS supercells.

$$F^{vib} = k_b T \int \ln[2\sinh(\hbar\omega/(2k_bT))]\, g(\omega) d\omega. \quad (11)$$

Assuming $g(\omega) = \sum_\alpha \delta(\omega - \omega_\alpha)$ (where the subscript α indicates the discrete modes calculated) this yields the expression used herein

$$F^{vib} = k_b T \sum_\alpha \ln[2\sinh(\hbar\omega_\alpha/(2k_bT))]. \quad (12)$$

D. Charged point defects calculation

According to Eq. (10), the formation energies of charged defects depend on μ_F because of charge transfer between the localized defect states and the rest of the system. For example, the formation energy of the singly charged Cu vacancy is $\Delta E_{V_{Cu}^-}(\mu_F)$. Therefore, the concentration of singly charged copper vacancies can be given as

$$[V_{Cu}^-] = [Cu_{Cu}] g_{V_{Cu}^-} \exp\left(-\frac{\Delta F^{vib}_{V_{Cu}^0}}{k_bT}\right) \exp\left(-\frac{\Delta E_{V_{Cu}^-}(\mu_f) + \mu_{Cu}}{k_bT}\right). \quad (13)$$

In this work, we assume that the changes in vibrational free energies for the neutral and charged defects are equal—i.e., that $\Delta F^{vib}_{V_{Cu}^0} = \Delta F^{vib}_{V_{Cu}^-}$.

Since the concentrations of the neutral defects were already determined, the concentrations of the charged acceptors and donors can be calculated according to Fermi-Dirac statistics[25]

$$[X_a^{z-}] = \frac{[X_a]}{(g_{X_a^{z-}}/g_{X_a^0})\exp[(\varepsilon_{X_a^{z-}} - \mu_F)/kT] + 1}, \quad (14)$$

$$[X_d^{z+}] = \frac{[X_d]}{(g_{X_d^{z+}}/g_{X_d^0})\exp[(\mu_F - \varepsilon_{X_d^{z+}})/kT] + 1}, \quad (15)$$

where $[X_a] \equiv [X_a^0] + [X_a^{z-}]$ and $[X_d] \equiv [X_d^0] + [X_d^{z+}]$ are the total concentrations of acceptor and donor-like defects, $[X_a^0]$ and $[X_d^0]$ are the concentrations of neutral defects, z is the charge state, μ_F is the Fermi energy, $\varepsilon_{X_a^{z-}}$ are the charge transition levels (from Ref. 13, reproduced in Table I), and $g_{X_a^{z-}}, g_{X_d^{z+}}$ are the degeneracy factors of the acceptors or donors, see Table I. It should be noted that calculation of the $g_{X_a^{z-}}$ and $g_{X_d^{z+}}$ requires very careful analysis of the many-body energy states of the defects as well as the single-particle band states.[56] However, the electronic structure of CZTS and especially the details of the defects' internal states have not yet been well studied. Also, the degeneracy factors are not well defined at higher defect concentrations where defects begin to interact. Therefore, in present work, we assume for now that the degeneracy factors are identical to those for shallow donors and acceptors in a semiconductor with a non-degenerate conduction band and a doubly degenerate valence band maximum, namely $g_{X_d^{z+}} = 0.5$ and $g_{X_a^{z-}} = 2$, see Table I. We note that Persson[57] has predicted that the three highest valence bands in CZTS and CZTSe are non-degenerate at Γ; however, we could not account for this without making unjustified assumptions for the defects' electronic states.

Using Eqs. (14) and the definitions for $[X_a]$ and $[X_d]$ above, the concentrations of charged defects are given by equations of the form (using V_{Cu}^- as a concrete example)

$$[V_{Cu}^-] = [V_{Cu}^0](g_{V_{Cu}^-}/g_{V_{Cu}^0})\exp\left(\frac{\mu_F - \varepsilon_{V_{Cu}^-}}{k_bT}\right). \quad (16)$$

The transition energy level of an acceptor or donor (e.g., $\varepsilon_{V_{Cu}^-}$ in the case of single charged copper vacancy) is equal to the energy difference $\varepsilon(q_1/q_2) = [\Delta E_{D,q_1} - \Delta E_{D,q_2}]/(q_2 - q_1)$ between the charge states q_1 and q_2 for the defect.[27] Therefore, Eq. (16) is equivalent to Eq. (13).

The general expressions for the concentrations of charged acceptors and donors are[22,23]

$$[X_a^{z-}] = [X_a^0](g_{X_a^{z-}}/g_{X_a^0})\exp\left(\frac{\mu_F - \varepsilon_{X_a^{z-}}}{k_bT}\right), \quad (17)$$

$$[X_d^{z+}] = [X_d^0](g_{X_d^{z+}}/g_{X_d^0})\exp\left(\frac{\varepsilon_{X_d^{z+}} - \mu_F}{k_bT}\right). \quad (18)$$

The concentration of free carriers from Fermi-Dirac statistics are[58,59]

$$n = \left(\frac{4\pi}{h^3}\right)(2m_e^*)^{3/2} \int_{E_c}^{\infty} \frac{(E - E_c)^{1/2}}{\left[1 + \exp\left(\frac{E - \mu_F}{k_bT}\right)\right]} dE, \quad (19)$$

$$p = \left(\frac{4\pi}{h^3}\right)(2m_p^*)^{3/2} \int_{-\infty}^{E_v} \frac{(E_v - E)^{1/2}}{\left[1 + \exp\left(\frac{\mu_F - E}{k_bT}\right)\right]} dE, \quad (20)$$

in which E_c *and* E_v are the energies of the conduction band minimum and valence band maximum and $m_{e(p)}$ is the density of states effective mass for electrons (holes). Density of states effective masses for electrons and holes were calculated from $m_{e(p)} = \sqrt[3]{2m_\perp^2 m_\parallel}$ to be $m_e = 0.186m_0$ and $m_p = 0.37m_0$, respectively, using the transverse $m_\perp$ and longitudinal $m_\parallel$ masses from Ref. 57.

If the Fermi level remains at least from a $3k_bT$ band edge then the computationally simpler Boltzmann statistics introduces negligible error. Thus, p and n may be computed from

$$p = N_v \exp\left(\frac{E_v - \mu_F}{kT}\right), \quad (21)$$

$$n = N_c \exp\left(\frac{\mu_F - E_c}{kT}\right), \quad (22)$$

in which $N_{c(v)} = 2\left(\frac{2\pi m_{e(p)} kT}{h^2}\right)^{3/2}$ is the effective density of states for the conduction (valence) band.

Finally, the Fermi energy μ_F, concentrations of charged defects, and concentrations of free carriers can be determined from self-consistently solving the equation of electroneutrality

$$p - n + \sum_i q[X_i^q] = 0, \tag{23}$$

in which X_i^q denotes the defect i in charge state q. In our model, this is given explicitly as

$$n + V_{Cu}^- + 2V_{Zn}^{2-} + Cu_{Zn}^- + 2Zn_{Sn}^{2-} = p + 2V_S^{2+} + Zn_{Cu}^+. \tag{24}$$

E. Full equilibrium and quenching

The point defect and free carrier densities can be calculated for cases of full equilibrium at the temperature of interest (such as annealing temperature) and after quenching (cooling of the material from high to the room temperature).[19,22] The procedure described above is used to compute the full equilibrium, while for quenching the total concentrations of defects are computed at high temperature as above and then the carrier and ionized defect concentrations are recomputed at a lower temperature.

III. RESULTS AND DISCUSSION

One of the most important issues in CZTS point defect analysis is a preliminary determination of limits within which the reference chemical potentials may change. In other words, it is necessary to define the boundary conditions for the reference chemical potentials in Eqs. (4)–(9). The values of the components' chemical potentials should be limited according to secondary phases and CZTS reaction formation, see Eqs. (25)–(30). The analysis of such reactions and estimation of the formation enthalpies ΔH at 0 K were performed in Ref. 13

$$\mu_{Cu} + \mu_S < \Delta H_{CuS} = -0.49\,\text{eV},^{13} \tag{25}$$

$$\mu_{Zn} + \mu_S < \Delta H_{ZnS} = -1.75,^{13} \tag{26}$$

$$\mu_{Sn} + \mu_S < \Delta H_{SnS} = -1.01\,\text{eV},^{13} \tag{27}$$

$$\mu_{Sn} + 2\mu_S < \Delta H_{SnS_2} = -1.33,^{13} \tag{28}$$

$$2\mu_{Cu} + \mu_{Sn} + 3\mu_S < \Delta H_{Cu_2SnS_3} = -2.36,^{13} \tag{29}$$

$$2\mu_{Cu} + \mu_{Zn} + \mu_{Sn} + 4\mu_S < \Delta H_{Cu_2ZnSnS_4} = -4.21.^{13} \tag{30}$$

However, the determination of the chemical potentials boundary conditions for high temperatures is more complicated, because formation enthalpies of the compounds depend on temperature. In addition, the formation enthalpies of the secondary phases of CZTS reported in Refs. 13–16 are significantly different. Also, the differences between calculated and experimentally determined formation enthalpy of compounds can still be large.[15] Therefore, formation enthalpies in Eqs. (25)–(30) should be considered only as approximate boundary conditions for the analysis of point defect equilibrium at high temperature. Lastly, since the chemical potentials, formation energies, and charge transition energies always appear together in the argument of the Boltzmann factors for defect formation probability, the variations of the chemical potentials in calculations may be used to absorb uncertainties in the calculated values of these input parameters. Therefore, in this work, we prefer to choose reasonable boundaries over which to vary the chemical potentials using the secondary phase formation constraints as guidance, as opposed to taking them as exact limits.

The estimation of the Cu, Zn, and Sn reference chemical potentials is rather difficult task because the equilibrium vapour pressures of metals during CZTS deposition or annealing are, in general, not known. On the contrary, the partial pressure of sulfur dimers P_{S_2} above pure sulfur has been measured carefully as a function of temperature,[60] hence its chemical potential μ_{S_2} can be determined from the ideal gas model,[51,52] see Eq. (B2). The elemental sulfur chemical potential appearing in the defect formation reactions was calculated as $\mu_S = 0.5\mu_{S_2}$ assuming no complications from surface reactions. The variation of the sulfur chemical potential and P_{S_2} pressure with annealing temperature according to experiment,[60] given by Eq. (B10), is shown in Fig. 2. As can be seen, the value of the sulfur chemical potential calculated for typical range of annealing temperature from 500 to 600 °C varies from −1.06 to −0.95 eV that is much lower than the values calculated in Refs. 13–16 using the sum rules derived from the computed formation enthalpies for CZTS. Also, in Refs. 13–16, the sulfur chemical potential was varied within a broad range from 0 to −0.72 eV, which corresponds to a drastic enhancement of the sulfur pressure, as compared to single-zone annealing conditions. Such extremely S-rich conditions could be achieved using sources at less negative chemical potentials than the CZTS (e.g., effusion cells at higher temperature or a plasma), but are impossible to achieve if the CZTS is in equilibrium with an elemental S source at the same temperature. This leads to one important finding of our work, namely that CZTS is expected to be heavily compensated and to have a vanishing minority carrier lifetime especially in one-zone prepared materials because of sulfur vacancies, which are predicted to result in mid-gap trap states.

Although we know that the chemical potential boundaries for the single-phase CZTS will be wider at higher temperatures, we use the more restrictive computed bounds as guidelines such that phase segregation should not occur upon cooling from the annealing temperatures. Relatively low values of the sulfur chemical potential allow variation in the Cu and Sn chemical potentials without violating the secondary phases formation conditions, see Eqs. (25)–(30). However, the value of Zn chemical potential cannot be varied in a broad range because of the low formation enthalpy for ZnS $\Delta H_{ZnS} = -1.75$ eV, see Eq. (26). For example, the Zn chemical potential at $T = 550$ °C should not exceed −0.75 eV as the sulfur chemical potential at this temperature is −1.0 eV. Given these guidelines, we have chosen the following reasonable ranges of chemical potentials for this work: μ_{Cu} from −0.7 to −0.1 eV, μ_{Zn} from −1 to −0.75 eV, and μ_{Sn} from −0.6 to −0.4 eV.

The vibrational properties of the CZTS crystal with different point defects are illustrated by the phDOS and its

modifications for each defect are shown in Fig. 3. We computed the phonon spectra for all Cu-related defects at both Cu sites in the kesterite unit cell and found that the differences are, even if not very remarkable, yet not negligible. A single most prominent difference is a split-off mode at 41 cm^{-1} occurring in the spectrum of supercell with the S vacancy. An inspection of vibration eigenvectors shows that these are, in fact, two almost degenerate modes, strongly localized on the 1st and 2nd neighbors of the vacancy. The impurity breaks four cation-anion zigzag chains running at different angles; notably, there are two chains -S-Cu-(vacancy)-Sn-S-, according to two Cu atoms neighboring the sulphur. The modes in question "live" exclusively on these chains: Cu and Sn "breath" around the vacancy, moving in opposite senses, and each cation is followed by its next neighboring sulphur (hence an acoustic character of this mode), beyond which the vibration dies out. The integration of the phDOS and Bose-Einstein occupation according to Eq. (12) determines the vibrational free energy for the perfect and defected supercells, and hence their difference ΔF^{vib}. Numerical values of ΔF^{vib} at 550 °C are listed in Table I. Further on, the vibrational term in Eqs. (4)–(9), which represents the multiplicative correction factor to the standard quasichemical calculation ignoring vibrational factors, was calculated as a function of temperature; it is shown in Fig. 4. It is important to note that this factor has different temperature dependences and magnitudes for different defects; therefore, the inclusion of the ΔF^{vib} correction factor to the final defect equilibrium has nontrivial effects.

As seen from Eq. (12), the value of the vibrational factor in the final defect concentrations $\exp\left(\frac{-\Delta F^{vib}}{k_B T}\right)$ (i.e., the quantity plotted in Fig. 4) is dependent on the sum over occupied modes as a function of temperature. Therefore, defects which shift spectral weight in the phDOS to lower frequencies (for example, the introduction of the new mode below 50 cm^{-1} by V_S^0) will have higher values of this factor at lower temperatures. For reference: room temperature corresponds to approximately 220 cm^{-1}, so defects which strongly modify the phDOS below this demarcation frequency will tend to have higher values of the vibrational factor.

The value of the vibrational modification to the final concentrations for the V_{Cu}^0 and Zn_{Sn}^0 defects is approximately 0.5 in the target temperature range for annealing (from 500 to 600 °C), is roughly an order of magnitude higher for Cu_{Zn}^0 and V_{Zn}^0, and is approximately 60 and 600 for the V_S^0 and Zn_{Cu}^0 defects, respectively. Thus, the vibrational term is non-negligible: it may modify the relative concentrations of the different defects in CZTS by 3–4 *orders of magnitude*. Hence, we believe that inclusion of the effects of vibrational free energy ΔF^{vib} from realistic phDOS calculations for each specific defect as opposed to questionable empirical power laws of temperature[22] is critical for quasichemical analysis of point defect equilibrium in all semiconductors now that such calculations are becoming feasible computationally.

The calculations of the sulfur chemical potential for the temperature range from 500 to 600 °C show that stable chemical-potential region of CZTS in equilibrium with saturated S equilibrium vapor is different as calculated at T = 0 K.[13] Also, it was determined that values of the vibrational energy terms in Eqs. (4)–(9) are substantial at finite temperatures for at least two enthalpically unfavored defects, namely V_S^0 and Zn_{Cu}^0 (Fig. 4). These important differences make it necessary to verify whether it is possible to adequately describe point defect equilibrium at high temperature for the stable chemical-potential region estimated for 0 K and negligible vibration terms (i.e., $\Delta F^{vib} = 0$ in Eqs. (4)–(9)). Such calculations were performed for full equilibrium ($T = 550$ °C) and quenching conditions using Eqs. (4)–(9) and Eqs. (17)–(20) and (24). Note that it is necessary to use full Fermi-Dirac statistics (Eqs. (19) and (20)) at the annealing temperature, since degenerate conditions are

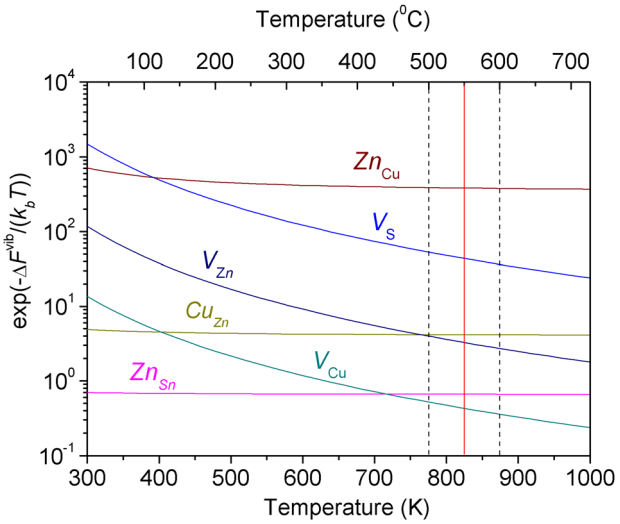

FIG. 4. The values of the vibrational term $\exp\left(\frac{-\Delta F^{vib}}{k_B T}\right)$ in the expressions for the neutral point defect concentrations for the defects considered in this work. Black dashed lines correspond to the usual temperature range for the CZTS films annealing and the red solid line corresponds to the 550 °C temperature at which most calculations of the point defect equilibrium were performed.

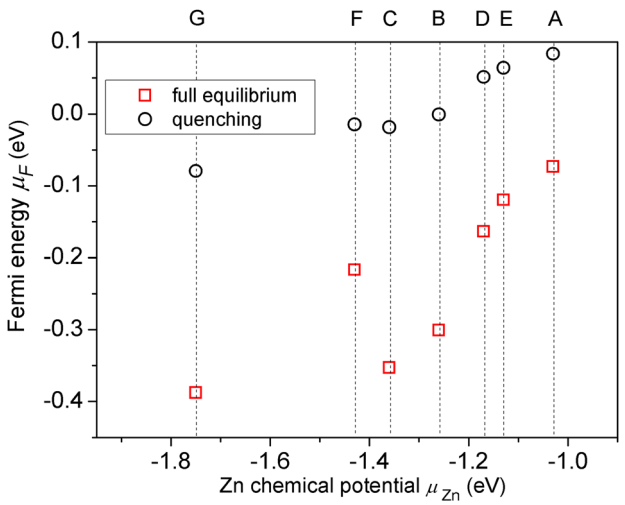

FIG. 5. The Fermi energy calculated for the different points (A, B, etc.) of the CZTS stable chemical potential region according to Ref. 13. The rectangles and circles correspond to full equilibrium at $T = 550$ °C and quenching to room temperature conditions, respectively. In this figure, the vibrational free energy ΔF^{vib} in Eqs. (4)–(9) was assumed to be zero to demonstrate its importance via the unreasonable predicted Fermi energy.

easily reached. The calculations were performed according to the stable chemical-potential region points determined in Ref. 13. As shown in Fig. 5, the calculations *without* the vibrational energy modification give results which are in conflict with experimental findings—namely they imply that CZTS should be nearly degenerately doped across a wide range of the metals' chemical potential space. Therefore, all following calculations of the high temperature point defect equilibrium were carried out taking into account the vibrational terms (Fig. 4) in Eqs. (4)–(9) and using the S equilibrium vapor chemical potential computed from experimental vapor pressure curves (Fig. 2).

The concentrations of neutral defects within a one-zone annealing model were calculated according to Eqs. (4)–(9) with inputs from Table I; the results are shown in Fig. 6. They indicate that Cu-related acceptor-like defects remain

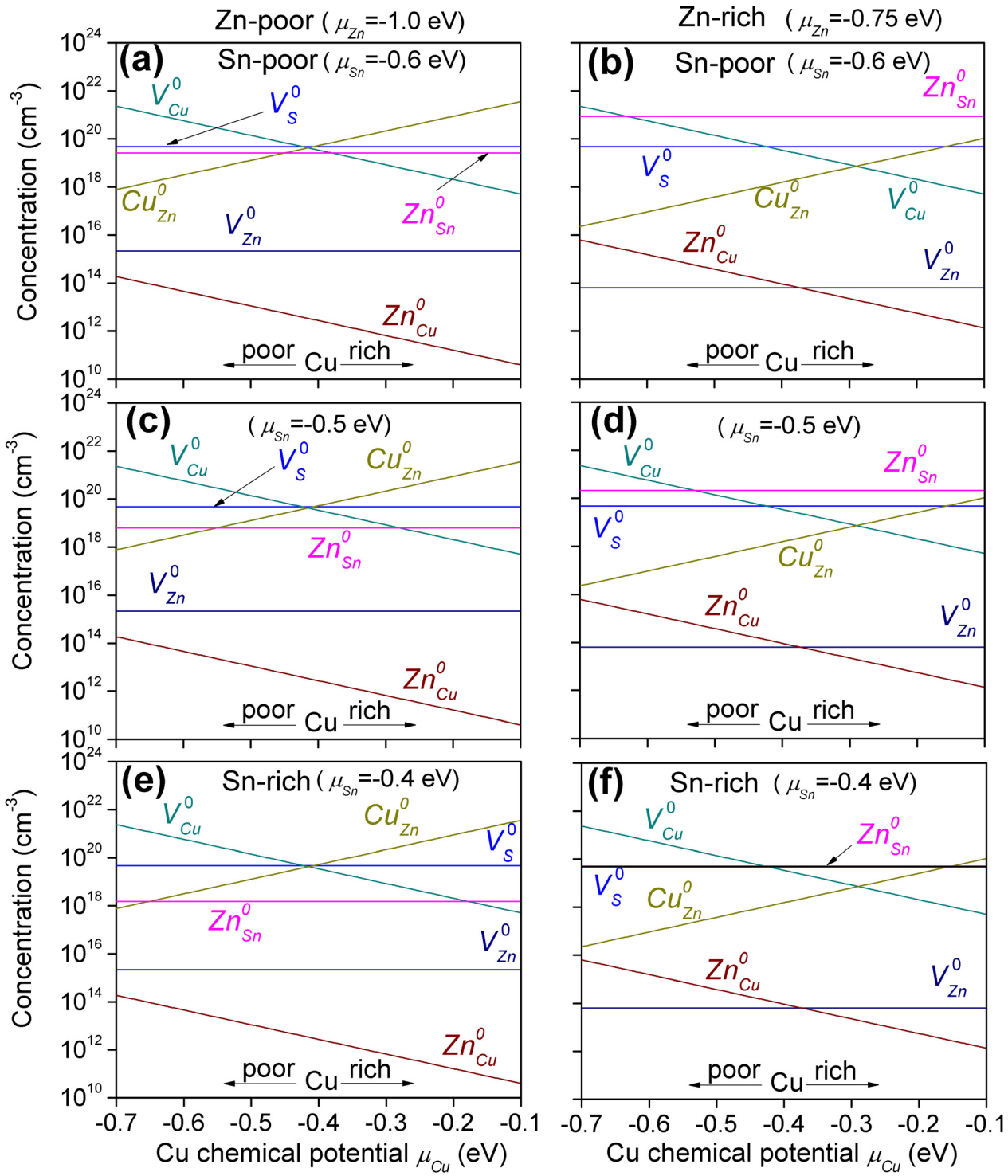

FIG. 6. Concentration of the neutral point defects of CZTS calculated for the constant sulfur chemical potential $\mu_S = -0.996$ eV and different fixed Zn and Sn chemical potentials as a function of Cu chemical potential under annealing temperature $T = 550\,^{\circ}$C and equilibrium S_2 vapor pressure $P_{S_2} = 1.2 \times 10^4$ Pa: (a), (c), and (e) Zn-poor conditions $\mu_{Zn} = -1$ eV; (b), (d), and (f) Zn-rich conditions $\mu_{Zn} = -0.75$ eV; (a) and (b) Sn-poor conditions $\mu_{Sn} = -0.6$ eV; (c) and (d) Sn-intermediate conditions $\mu_{Sn} = -0.5$ eV; (e) and (f) Sn-rich conditions $\mu_{Sn} = -0.4$ eV.

dominant for all reasonable chemical potential values (unsurprisingly in light of their extremely low formation energies, see Ref. 13), so that when one type of defect's concentration is suppressed, another's is enhanced. Also, intuitively, Zn-rich and Sn-poor conditions may lead to large concentrations of Zn^0_{Sn}. However, intuition breaks down for defects such as V^0_{Zn}at Zn-poor conditions—Fig. 6 shows that this defect is not formed in large concentrations despite Zn-deficiency. In Figure 6, the concentration of the neutral sulfur vacancy V^0_S is constant in each panel for fixed μ_{Zn}, since the annealing temperature is kept constant. However, as shown in Fig. 6, in the intermediate range of Cu chemical potentials V^0_S becomes one of the dominating defects as the net acceptor concentration decreases. This may have severe implications for one-

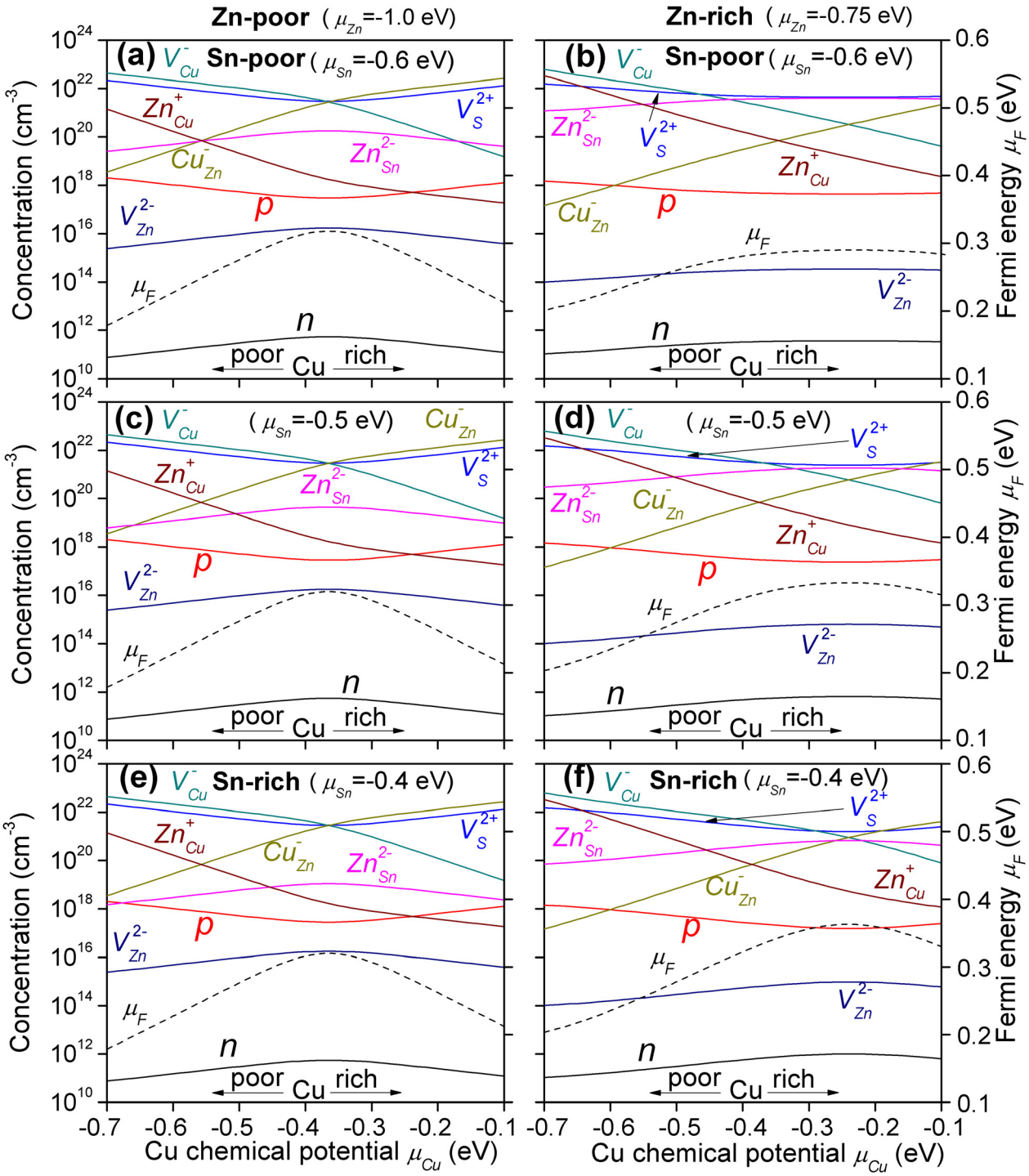

FIG. 7. Concentration of the charged point defects and Fermi energy of CZTS as a function of components chemical potentials at full equilibrium conditions calculated for the constant sulfur chemical potential $\mu_S = -0.996$ eV and different fixed Zn and Sn chemical potential as a function of Cu chemical potentials under annealing temperature $T = 550\,^\circ$C and equilibrium S_2 vapor pressure $P_{S_2} = 1.2 \times 10^4$ Pa: (a), (c), and (e) Zn-poor conditions $\mu_{Zn} = -1$ eV; (b), (d), and (f) Zn-rich conditions $\mu_{Zn} = -0.75$ eV; (a) and (b) Sn-poor conditions $\mu_{Sn} = -0.6$ eV; (c) and (d) Sn-intermediate conditions $\mu_{Sn} = -0.5$ eV; (e) and (f) Sn-rich conditions $\mu_{Sn} = -0.4$ eV.

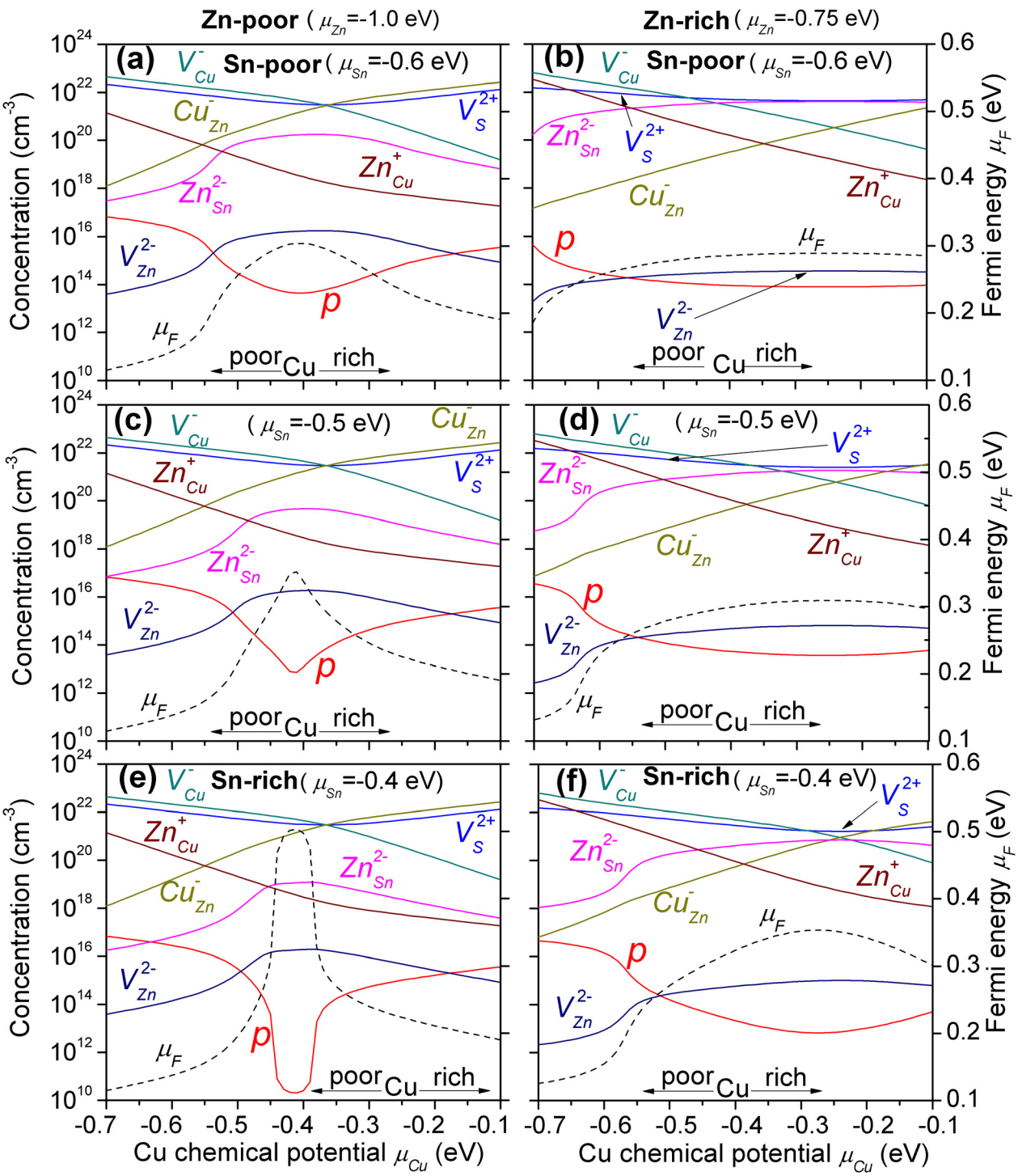

FIG. 8. Concentration of the charged point defects and Fermi energy of CZTS after the quenching from 550 °C to 27 °C as a function of components chemical potentials calculated for the constant sulfur chemical potential $\mu_S = -0.996$ eV and different fixed Zn and Sn chemical potential as a function of Cu chemical potentials under annealing temperature $T = 550$ °C and diatomic sulfur pressure $P_{S_2} = 1.2 \times 10^4$ Pa: (a), (c), and (e) Zn-poor conditions $\mu_{Zn} = -1$ eV; (b), (d), and (f) Zn-rich conditions $\mu_{Zn} = -0.75$ eV; (a) and (b) Sn-poor conditions $\mu_{Sn} = -0.6$ eV; (c) and (d) Sn-intermediate conditions $\mu_{Sn} = -0.5$ eV; (e) and (f) Sn-rich conditions $\mu_{Sn} = -0.4$ eV.

zone annealed CZTS, because this defect is predicted to introduce mid-gap charge transition levels which could act as effective recombination centers.

The calculation of charged point defects must include solving self-consistently the system of Eqs. (17)–(20) including electrons and holes, varying the μ_i first for the full equilibrium conditions and then for the quenching. Note that the free carrier concentrations n and p were calculated with Fermi-Dirac statistics for full equilibrium (high temperature conditions), but with Boltzmann statistics for the final free carrier concentrations at room temperature for quenching. This was done for computational efficiency and at room temperature the assumption of non-degeneracy was always satisfied. Ionized defect concentrations were always computed from Fermi-Dirac statistics for accuracy.

Figure 7 shows the predicted concentrations of defects for full equilibrium at the representative annealing temperature of 550 °C for different combinations of chemical potentials. The plotted curves represent the concentrations of the defects which would be observed using *in situ* measurements (e.g., high-temperature Hall effect) during film processing. It is seen that the V_{Cu}^{-}, Cu_{Zn}^{-}, and V_S^{2+} defects are dominant, similar to their neutral counterparts (Fig. 6), for all reasonable chemical potential values. These defects thus mainly determine μ_F and hence the free carrier concentration for most chemical potential ranges. Other defects have lower concentrations but may act as traps and recombination centers and thus drastically influence the minority carrier lifetime, which is critical for device performance. Zn-rich conditions promote the formation of Zn_{Sn}^{2-} as well as Zn_{Cu}^{+} compensating donors, as seen in Figs. 7(b), 7(d) and 7(f). Moreover, Zn_{Sn}^{2-} is dominant at Zn-rich and Sn-poor conditions—see Fig. 7(b). As one of the two acceptors V_{Cu}^{-} or Cu_{Zn}^{-} is always dominant, the total acceptor concentration changes insignificantly over the range of chemical potentials we considered. However, the hole density p is many orders of magnitude lower because of the very high (99.99%) compensation ratio. This results in a weak dependence of the net hole concentration on μ_{Cu}; p varies slightly around $10^{17}\,cm^{-3}$ across a range of conditions. The maximum of μ_F (lowest hole concentration) is observed at intermediate values of μ_{Cu} when the concentrations of the V_{Cu}^{-} and Cu_{Zn}^{-} acceptors are minimal and the compensation effect caused by V_S^{2+} and Zn_{Cu}^{2+} donors becomes more pronounced. The doubly charged V_S^{2+} provide the major contribution to the compensation of acceptors in this range. The maximum value of μ_F (about 0.37 eV) corresponds to Zn-rich and a Sn-rich condition, see Fig. 7(f), and becomes slightly smaller under Zn-poor, see Figs. 6(a), 6(c) and 6(e), Zn-rich Sn-poor conditions, see Fig. 7(b), as well as under Zn-rich and Sn-intermediate conditions, see Fig. 7(d).

The results of charged point defect calculations for quenching—i.e., holding the total point defect concentrations computed at the annealing temperature constant but recomputing charge carrier and defect ionization statistics at room temperature–are presented in Fig. 8. The quenched model predicts a drastic decrease of the free carrier concentrations by $>10^{3}\,cm^{-3}$ for the hole concentration. The general trends in the hierarchy of point defect concentrations remain similar to those in full equilibrium temperature regime. Namely, the ionized V_{Cu}^{-}, Cu_{Zn}^{-}, and V_S^{2+} defects remain dominant for different values of the chemical potentials because of their large total concentrations and, in the case of acceptors, because of their relatively low ionization energies. However, the effect of the Zn-related antisites Zn_{Sn}^{2-} and Zn_{Cu}^{+} on free carrier concentrations is much more significant under quenched conditions. The high concentration of Zn_{Sn}^{2-} under Zn-rich conditions, see Figs. 8(b), 8(d) and 8(f), provides comparatively small changes of μ_F around 0.3 eV within broad range of μ_{Cu} from −0.1 to −0.5 eV. A decrease in μ_F (higher hole concentration) is observed only for low $\mu_{Cu} < -0.55$ eV. Under Zn-poor conditions, see Figs. 8(a), 8(c) and 8(e), concentration of Zn_{Sn}^{2-} decreases leading to very high compensation due to Zn_{Cu}^{+} and V_S^{2+} donors. This effect becomes more pronounced with increase of μ_{Sn} and hence decreases of the Zn_{Sn}^{2-} concentration. For example, μ_F is changed from 0.32 to 0.52 eV with μ_{Sn} increasing from −0.6 to −0.5 eV at the same Cu-chemical potential of −0.4 eV.

Given these observations, it is clear that varying μ_{Zn} and μ_{Sn} rather than μ_{Cu} will lead to more significant changes in the net hole concentration (at least under one-zone processing conditions using elemental S as the S source). These observations are in a good agreement with experimental results by some of us in Ref. 47 which demonstrated strong influence of the [Zn]/[Sn] ratio on the conductivity value of the CZTS thin films, whereas the influence of the variation of the [Cu]/([Zn] + [Sn]) ratio was much less evident (note that intragrain doping also influences the grain boundary barriers for a given interface trap density by modifying the built-in potential).

Finally, we note that the following amendments may be necessary to improve the current model. (1) The refinement of theoretical defect formation energies and charge transition values especially with inputs from experiment. (2) The inclusion of defect complexes: it is expected that many different defect complexes may form and modify the relations between lattice imperfections and carrier concentrations. (3) As computational resources and algorithms improve, the phonon spectra should be recalculated for increasingly larger supercells to minimize artifacts from finite size effects. We note, however, that in view of large concentrations predicted for some defects, smaller supercells may in fact be more accurate. Ideally, the vibrational and electronic computations should include the effects of disorder induced by defects. (4) The boundaries of the single phase CZTS region as functions of chemical potentials and temperature should be more precisely experimentally established. Furthermore, it is widely believed that some Zn-rich films contain intragranular ZnS-like (or at least more insulating) regions; it has been demonstrated that ZnS may form either at the front or back interfaces of the films. (5) Thus, the computation of defect equilibrium in CZTS should also include the possibility of two-phase equilibrium with—at least—ZnS, but ideally also including other secondary phases such as Cu_2SnS_3.

IV. CONCLUSIONS

We report a quasichemical model capable of calculating the native point defect equilibrium and free carrier concentrations in CZTS for a variety of experimental conditions. It was determined that the influence of the changes in phDOS induced by defects may substantially affect the concentration of defects through the vibrational free energy—especially in the cases of V_S and Zn_{Cu} amongst the defects we considered. This suggests that future works on point defect equilibrium in semiconductors should take into account the defect-induced modifications to the phonon spectrum since it can significantly affect the predicted concentrations especially at high temperatures.

Calculation of the point defect concentrations for one-zone annealing with elemental sulfur as the chalcogen source shows that V_{Cu}^{-}, Cu_{Zn}^{-}, and V_S^{2+} are the dominant defects across a large range of chemical potentials. The sulfur

vacancies are predicted to be a very significant source of compensation and possibly recombination in this type of sample preparation, but supplying S at higher chemical potential could be effective in suppressing them. We note that for both quenched and full-equilibrium conditions, the predicted hole concentrations are many orders of magnitude lower than the net defect concentrations which has significant implications for how the bulk band structure of CZTS is treated. Strong disorder effects and band tailing are to be expected in such heavily compensated semiconductors.

Under Zn-poor conditions, V_{Cu}^{-}, Cu_{Zn}^{-}, and V_S^{2+} defects determine the doping and compensation in CZTS. At intermediate values of μ_{Cu} near -0.4 eV, when $[V_{Cu}^{-}] + [Cu_{Zn}^{-}] \approx [V_S^{2+}]$, the maximal compensation occurs and hence the Fermi level is shifted towards midgap. Under such conditions, Zn_{Sn}^{2-} has a pronounced effect on the Fermi level. This was seen through variation of μ_{Sn} at constant μ_{Cu}, μ_{Zn}, and μ_S, which lead to drastic changes in Fermi energy of about 0.3–0.5 eV when chemical composition is shifted from Sn-poor to Sn-rich conditions. Based on these results, we speculate that Cu-poor coupled with either too Zn-rich or too Sn-rich conditions should lead to heavily compensated CZTS, which is unsuitable for solar cells applications. Under Zn-rich conditions, the net hole concentration changes little with Cu chemical potential due to the dominance of V_{Cu}^{-} for Cu-poor conditions and Cu_{Zn}^{-} and Zn_{Sn}^{2-} for Cu-rich conditions and the near-constant V_S^{2+} concentration. For Zn-rich conditions, the net hole concentration can be efficiently controlled by the variation of μ_{Sn} and μ_{Zn}, but it remains rather insensitive to μ_{Cu}. Considerable increases in hole concentration are observed only for excessive Cu-poorness, $\mu_{Cu} < -0.6$ eV. These model predictions are compatible with the widely reported necessity for Cu-poor conditions combined with a certain optimal range of Zn-rich conditions. This required optimal Zn-richness may at least in part be a manifestation of the need to suppress compensation by both V_S^{2+} and Zn_{Cu}^{+} donors, although it is also possible that the presence of an optimal volume fraction of ZnS precipitates or ZnS-like intragrain regions may also be beneficial to cell performance.

Cu-related defects (V_{Cu}^{-} and Cu_{Zn}^{-}) are dominant over a broad range of CZTS chemical potential space. These defects provide a high, nearly constant concentration of acceptors. This is in accord with the findings based solely on formation enthalpies.[13–16] However, our calculations show that for one-zone annealing V_S^{2+} and Zn_{Cu}^{+} should also occur in large numbers and provide high compensation as well as deep states. To fully understand the fluctuating potentials, compensation, and defect related recombination in CZTS, full consideration of finite temperature effects is required.

In final summary, our approach allows us to investigate point defect and carrier concentrations in CZTS in various sample processing conditions and to gain insight into the relationships amongst processing parameters and defect densities. The calculational framework is generalizable to any semiconductor and is open to technical improvements resulting from progress in state-of-the-art electronic structure and phonon calculations.

ACKNOWLEDGMENTS

We thank Dr. Shiyou Chen for sharing the numerical values of the charge transition energies from Ref. 13. The work at the University of Utah was supported in full by the U.S. Department of Energy, Office of Basic Energy Sciences, Division of Materials Sciences and Engineering under Award No. DE-SC0001630. Calculations of vibration spectra have been done using the facilities of the PMMS at the University of Lorraine.

APPENDIX A: CALCULATION OF CONCENTRATIONS OF NEUTRAL POINT DEFECTS

We include herein a derivation of the quasichemical framework used in this paper as a reference for future works on multinary semiconductors. We have considered the components in Eq. (2) as grand canonical ensembles. Then, the chemical potentials of the perfect and defected CZTS crystal can be expressed via the total energy of the perfect E_i^t and defected primitive unit cell E_j^t correspondingly

$$\mu^t_{Cu_2ZnSnS_4} = k_bT \ln N_{Cu_2ZnSnS_4} - k_bT \ln \sum_{i=1}^{i=N_{Cu_2ZnSnS_4}} \Omega_i \times \exp\left(-\frac{E_i^t}{k_bT}\right), \tag{A1}$$

$$\mu^t_{CuV^0_{Cu}ZnSnS_4} = k_bT \ln N_{CuV^o_{Cu}ZnSnS_4} - k_bT \ln \sum_{j=1}^{j=N_{CuV^o_{Cu}ZnSnS_4}} \Omega_j \times \exp\left(-\frac{E_j^t}{k_bT}\right). \tag{A2}$$

Here, $N_{Cu_2ZnSnS_4}$ and $N_{CuV^o_{Cu}ZnSnS_4}$ are the numbers of perfect primitive CZTS unit cells and those with a copper vacancy; Ω_i and Ω_j are the degeneracies of the i and j states correspondingly

The copper vapor phase can be described with the help of the ideal gas approximation. In this case, the chemical potentials of the copper gas can be expressed in terms of the total energy of each individual copper atom ε_k^t

$$\mu^t_{Cu} = k_bT \ln N_{Cu} - k_bT \ln \sum_{k=1}^{k=N_{Cu}} \omega_k \exp\left(-\frac{\varepsilon_k^t}{k_bT}\right), \tag{A3}$$

where N_{Cu} is the number of Cu atoms in the gas phase, ε_k^t is the total energy of a copper atom in the gas phase, and ω_k is the degeneracy of the k state.

The total energy of any component can be given as

$$E^t = E^{vibr} + E^{trans} + E^{rot} + E^0, \tag{A4}$$

in which $E^{vibr}, E^{trans}, E^{rot}$, and E^0 are the vibration, translational, rotational, and electronic self energies.

Taking into account that for the solid state $E^{trans} = E^{rot} = 0$ and for the monatomic gas $\varepsilon^{vib} = \varepsilon^{rot} = 0$, the total energies of perfect primitive unit cell, defected primitive unit cell, and a copper atom in the gas phase can be

expressed according to Eq. (A4) as $E_i^t = E_i^{vibr} + E_i^0$ $E_j^t = E_j^{vibr} + E_j^0$, and $\varepsilon_k^t = \varepsilon_k^{trans} + \varepsilon_k^0$. Evaluating Eqs. (A1)–(A4) yields

$$\mu^t_{Cu_2ZnSnS_4} = k_bT \ln N_{Cu_2ZnSnS_4} - k_bT \ln \sum_{i=1}^{i=N_{Cu_2ZnSnS_4}} \Omega_i^{vibr} \times \exp\left(-\frac{E_i^{vibr}}{k_bT}\right)\Omega_i^0 \exp\left(-\frac{E_i^0}{k_bT}\right), \quad (A5)$$

$$\mu^t_{CuV^0_{Cu}ZnSnS_4} = k_bT \ln N_{CuV^o_{Cu}ZnSnS_4} - k_bT \ln \sum_{j=1}^{j=N_{CuV^o_{Cu}ZnSnS_4}} \Omega_j^{vibr} \times \exp\left(-\frac{E_j^{vibr}}{k_bT}\right)\Omega_j^0 \exp\left(-\frac{E_j^0}{k_bT}\right), \quad (A6)$$

$$\mu^t_{Cu} = k_bT \ln N_{Cu} - k_bT \ln \sum_{k=1}^{k=N_{Cu}} \omega_k^{trans} \exp\left(-\frac{\varepsilon_k^{trans}}{k_bT}\right)\omega_k^0 \times \exp\left(-\frac{\varepsilon_k^0}{k_bT}\right). \quad (A7)$$

The vibrational partition functions can be written as

$$Z^{vibr}_{Cu_2ZnSnS_4} = \sum_{i=1}^{i=N_{Cu_2ZnSnS_4}} \Omega_i^{vibr} \exp\left(-\frac{E_i^{vibr}}{k_bT}\right), \quad (A8)$$

$$Z^{vibr}_{CuV^0_{Cu}ZnSnS_4} = \sum_{j=1}^{j=N_{CuV^o_{Cu}ZnSnS_4}} \Omega_j^{vibr} \exp\left(-\frac{E_j^{vibr}}{k_bT}\right), \quad (A9)$$

in which $Z^{vibr}_{Cu_2ZnSnS_4}$ and $Z^{vibr}_{CuV^0_{Cu}ZnSnS_4}$ are the vibrational partition functions of perfect CZTS crystal and a CZTS crystal with copper vacancies V^0_{Cu}, respectively.

The self energy term was obtained by summing over i, j, k

$$\sum_{j=1}^{j=N_{CuV^o_{Cu}ZnSnS_4}} \Omega_j^0 \exp\left(-\frac{E_j^0}{k_bT}\right) = \Omega^0_{Cu_2ZnSnS_4} \exp\left(-\frac{E^0_{Cu_2ZnSnS_4}}{k_bT}\right), \quad (A10)$$

$$\sum_{j=1}^{j=N_{CuV^o_{Cu}ZnSnS_4}} \Omega_j^0 \exp\left(-\frac{E_j^0}{k_bT}\right) = \Omega^0_{CuV^0_{Cu}ZnSnS_4} \times \exp\left(-\frac{E^0_{CuV^0_{Cu}ZnSnS_4}}{k_bT}\right), \quad (A11)$$

$$\sum_{k=1}^{k=N_{Cu}} \omega_k^0 \exp\left(-\frac{\varepsilon_k^0}{k_bT}\right) = \omega^0_{Cu} \exp\left(-\frac{\varepsilon^0_{Cu}}{k_bT}\right), \quad (A12)$$

where $E^0_{Cu_2ZnSnS_4}$, $E^0_{CuV^0_{Cu}ZnSnS_4}$, and ε^0_{Cu} are the reference energies of the perfect CZTS crystal, CZTS crystal with copper vacancies V^0_{Cu}, and copper atoms in a gas phase, respectively; $\Omega^0_{Cu_2ZnSnS_4}$, $\Omega^0_{CuV^0_{Cu}ZnSnS_4}$, and ω^0_{Cu} are the degeneracies of the $E^0_{Cu_2ZnSnS_4}$, $E^0_{CuV^0_{Cu}ZnSnS_4}$, and ε^0_{Cu} energies, correspondingly. Note that we assumed that the $E^0_{Cu_2ZnSnS_4}$, $E^0_{CuV^0_{Cu}ZnSnS_4}$, and ε^0_{Cu} energy levels are nondegenerate, hence $\Omega^0_{Cu_2ZnSnS_4} = \Omega^0_{CuV^0_{Cu}ZnSnS_4} = \omega^0_{Cu} = 1$. Substituting Eqs. (A8)–(A12) into Eqs. (A5)–(A7) results in

$$\mu^t_{Cu_2ZnSnS_4} = k_bT \ln N_{Cu_2ZnSnS_4} - k_bT \ln Z^{vibr}_{Cu_2ZnSnS_4} - k_bT \ln \Omega^0_{Cu_2ZnSnS_4} + E^0_{Cu_2ZnSnS_4}, \quad (A13)$$

$$\mu^t_{CuV^0_{Cu}ZnSnS_4} = k_bT \ln N_{CuV^o_{Cu}ZnSnS_4} - k_bT \ln Z^{vibr}_{CuV^0_{Cu}ZnSnS_4} - k_bT \ln \Omega^0_{CuV^0_{Cu}ZnSnS_4} + E^0_{CuV^0_{Cu}ZnSnS_4}, \quad (A14)$$

$$\mu^t_{Cu} = k_bT \ln N_{Cu} - k_bT \ln \sum_{k=1}^{k=N_{Cu}} \omega_k^{trans} \exp\left(-\frac{\varepsilon_k^{trans}}{k_bT}\right) - k_bT \ln \omega^0_{Cu} + \varepsilon^0_{Cu}. \quad (A15)$$

The vibrational free energy F^{vib} can be expressed through the vibrational partition function as: $F^{vib} = -k_bT \ln Z^{vib}$. Also, the translational chemical potential of the copper gas Eq. (A15) is given as $\mu^{trans}_{Cu} = \mu_{Cu} = k_bT \ln N_{Cu} - k_bT \ln \sum_k \omega_k^{trans} \exp\left(-\frac{\varepsilon_k^{trans}}{k_bT}\right)$ (here, we denote $\mu^{trans}_{Cu} = \mu_{Cu}$ for simplicity), which gives

$$\mu^t_{Cu_2ZnSnS_4} = k_bT \ln N_{Cu_2ZnSnS_4} + F^{vib}_{Cu_2ZnSnS_4} - k_bT \ln \Omega^0_{Cu_2ZnSnS_4} + E^0_{Cu_2ZnSnS_4}, \quad (A16)$$

$$\mu^t_{CuV^0_{Cu}ZnSnS_4} = k_bT \ln N_{CuV^o_{Cu}ZnSnS_4} + F^{vib}_{CuV^0_{Cu}ZnSnS_4} - k_bT \ln \Omega^0_{CuV^0_{Cu}ZnSnS_4} + E^0_{CuV^0_{Cu}ZnSnS_4}, \quad (A17)$$

$$\mu^t_{Cu} = \mu_{Cu} - k_bT \ln \omega^0_{Cu} + \varepsilon^0_{Cu}. \quad (A18)$$

Equations (A16)–(A18) should be substituted into Eq. (2) taking into account that $(\Omega^0_{CuV^0_{Cu}ZnSnS_4}\omega^0_{Cu})/\Omega^0_{Cu_2ZnSnS_4} = g_{V^0_{Cu}} = 1$ is the degeneracy of the neutral Cu vacancy V^0_{Cu}, and that the total concentration of copper lattice sites in the CZTS crystal $[Cu_{Cu}]$ is $1.248 \times 10^{22}\,\mathrm{cm}^{-3}$ for CZTS (not differentiating the two crystallographically distinct sites in kesterite).

Thus, the concentration of neutral Cu vacancies can be calculated as

$$[V^0_{Cu}] = [Cu_{Cu}] \exp\left(-\frac{F^{vib}_{CuV^0_{Cu}ZnSnS_4} - F^{vib}_{Cu_2ZnSnS_4}}{k_bT}\right) \times \exp\left(-\frac{E^0_{Cu_2V^0_{Cu}ZnSnS_4} - E^0_{Cu_2ZnSnS_4} + \varepsilon^0_{Cu} + \mu_{Cu}}{k_bT}\right) g_{V^0_{Cu}}. \quad (A19)$$

Finally, taking into account that $\Delta E_{V^0_{Cu}} = E^0_{Cu_2V^0_{Cu}ZnSnS_4} - E^0_{Cu_2ZnSnS_4} + \varepsilon^0_{Cu}$ is the free energy of point defect formation and that the difference in vibrational free energy between a

defective crystal and perfect crystal was denoted as $\Delta F^{vib}_{V^0_{Cu}} = F^{vib}_{Cu V^0_{Cu} ZnSnS_4} - F^{vib}_{Cu_2 ZnSnS_4}$ the concentration of copper vacancies may be reduced to

$$[V^0_{Cu}] = [Cu_{Cu}]\exp\left(-\frac{\Delta F^{vib}_{V^0_{Cu}}}{k_bT}\right)\exp\left(-\frac{\Delta E_{V^0_{Cu}} + \mu_{Cu}}{k_bT}\right) g_{V^0_{Cu}}. \tag{A20}$$

It should be noted that Eq. (A20) is typical for the neutral point defects calculations.[22,23]

APPENDIX B: SULFUR CHEMICAL POTENTIAL

Sulfur is known to evaporate as multiple species from S_2 dimers to S_8 rings. The equilibrium vapor becomes more dominated by S_2 as the temperature increases, and it is also clear that the S_2 dimers should be amongst the most reactive species. We thus assume herein that S_2 is the relevant active species at the annealing temperatures considered. The total chemical potential of diatomic sulfur can be expressed with the help of the total energy of the molecule[19,49,51] in analogy with Eq. (A3)

$$\mu^t_{S_2} = k_bT\ln N_{S_2} - k_bT\ln\sum_{l=1}^{l=N_{S_2}} \omega_l \exp\left(-\frac{\varepsilon^t_l}{k_bT}\right). \tag{B1}$$

However, in order to calculate the total energy of the diatomic sulfur molecule $\varepsilon^t_l = \varepsilon^{vibr}_l + \varepsilon^{trans}_l + \varepsilon^{rot}_l + \varepsilon^0_l$, it is necessary to consider vibrational and rotational energies as well as translational and the reference "self" energy

$$\mu^t_{S_2} = k_bT\ln N_{S_2} - k_bT\ln\sum_{l=1}^{l=N_{S_2}} \omega_l \exp\left(-\frac{\varepsilon^{trans}_l}{k_bT}\right)\exp\left(-\frac{\varepsilon^{rot}_l}{k_bT}\right) \times\exp\left(-\frac{\varepsilon^{vibr}_l}{k_bT}\right)\exp\left(-\frac{\varepsilon^0_l}{k_bT}\right). \tag{B2}$$

The energies may expressed with individual molecular partition functions[51]

$$z^{trans}_{S_2} = \sum_{l=1}^{l=N_{S_2}} \omega^{trans}_l \exp\left(-\frac{\varepsilon^{trans}_l}{k_bT}\right) = V\left(\frac{2\pi m_{S_2} k_bT}{h^2}\right)^{3/2}, \tag{B3}$$

$$z^{vib}_{S_2} = \sum_{l=1}^{l=N_{S_2}} \omega^{vib}_l \exp\left(-\frac{\varepsilon^{vibr}_l}{k_bT}\right) = \frac{\exp\left(\frac{-\theta_V}{2T}\right)}{1-\exp\left(\frac{-\theta_V}{T}\right)}, \tag{B4}$$

$$z^{rot}_{S_2} = \sum_{l=1}^{l=N_{S_2}} \omega^{rot}_l \exp\left(-\frac{\varepsilon^{rot}_l}{k_bT}\right) = \frac{T}{\sigma\theta_r}\left(1+\frac{1}{3}\frac{\theta_r}{T}+\frac{1}{15}\frac{\theta^2_r}{T^2}\right), \tag{B5}$$

in which $V = (N_{S_2}k_bT)/P_{S_2}$ is the volume, h is the Planck constant, m_{S_2} is the mass of a S_2 dimer, $\theta_V = 0.424\,\mathrm{K}$ and $\theta_r = 1040\,\mathrm{K}$ are the vibrational and rotational characteristic temperatures, and $\sigma = 2$ is the symmetry number.[19]

The chemical potential of S_2 dimers is obtained by substituting Eqs. (B3)–(B5) into Eq. (B2)

$$\mu^t_{S_2} = k_bT\ln N_{S_2} - k_bT\ln\left(z^{trans}_{S_2} z^{vibr}_{S_2} z^{rot}_{S_2}\right) - k_bT\ln\omega^0_{S_2} + \varepsilon^0_{S_2}. \tag{B6}$$

Assuming that $\mu^t_S = \frac{1}{2}\mu^t_{S_2}$ and $\varepsilon^0_S = \frac{1}{2}\varepsilon^0_{S_2}$, its chemical potential can be written as

$$\mu^t_S = \frac{1}{2}\mu^t_{S_2} = \frac{1}{2}\left(k_bT\ln N_{S_2} - k_bT\ln\left(z^{trans}_{S_2} z^{vibr}_{S_2} z^{rot}_{S_2}\right)\right) - \frac{1}{2}k_bT\ln\omega^0_{S_2} + \frac{1}{2}\varepsilon^0_{S_2}, \tag{B7}$$

$$\mu^t_S = \frac{1}{2}\left(k_bT\ln N_{S_2} - k_bT\ln\left(z^{trans}_{S_2} z^{vibr}_{S_2} z^{rot}_{S_2}\right)\right) - k_bT\ln\omega^0_S + \varepsilon^0_S. \tag{B8}$$

By analogy with Eq. (A12), the self-energy of the sulfur atom ε^0_S should be considered as part of the energy of neutral point defect formation and the $-k_bT\ln\omega^0_S$ term related to the degeneracy of sulfur atom energy levels should be included in the expression for the degeneracy of neutral sulfur vacancy, see Eqs. (A16)–(A18).

Thereby, chemical potential of the sulfur gas in Eq. (9) can be expressed according to Eqs. (B3)–(B5) as

$$\mu_S = \frac{1}{2}k_bT\left(\ln\left(\frac{P_{S_2}}{k_bT}\left(\frac{h^2}{2\pi m_{S_2}k_bT}\right)^{\frac{3}{2}}\right) - \ln\left(\frac{\exp\left(\frac{-\theta_V}{2T}\right)}{1-\exp\left(\frac{-\theta_V}{T}\right)}\right) - \ln\left(\frac{T}{\sigma\theta_r}\left(1+\frac{1}{3}\frac{\theta_r}{T}+\frac{1}{15}\frac{\theta^2_r}{T^2}\right)\right)\right). \tag{B9}$$

The experimental data[60] for the equilibrium partial pressure of S_2 above pure sulfur were fit to yield the semi-empirical expression

$$\log P_{S_2}(Pa) = -\frac{4928.53}{T} + 10.07. \tag{B10}$$

Thus, according to Eq. (B2), the chemical potential of sulfur may be expressed as a function of temperature only.

[1] D. B. Mitzi, O. Gunawan, T. K. Todorov, K. Wang, and S. Guha, Sol. Energy Mater. Sol. Cells **95**, 1421 (2011).
[2] H. Katagiri, K. Jimbo, and W. S. Ma, Thin Solid Films **517**, 2455 (2009).
[3] V. Fthenakis, Renewable Sustainable Energy Rev. **13**, 2746 (2009).
[4] T. E. Graedel, Annu. Rev. Mater. Res. **41**, 323 (2013).
[5] B. Shin, O. Gunawan, Y. Zhu, N. A. Bojarczuk, S. J. Chey, and S. Guha, Prog. Photovoltaics **21**, 72 (2013).
[6] T. K. Todorov, J. Tang, S. Bag, O. Gunawan, T. Gokmen, Y. Zhu, and D. B. Mitzi, Adv. Energy Mater. **3**, 34 (2013).
[7] J. Scragg, *Copper Zinc Tin Sulfide Thin Films for Photovoltaics, Synthesis and Characterisation by Electrochemical Methods*, Springer Theses (Springer, Berlin, 2011), p. 144.
[8] J. Just, D. Lutzenkirchen-Hecht, R. Frahm, S. Schorr, and T. Unold, Appl. Phys. Lett. **99**, 262105 (2011).
[9] S. Chen, X. G. Gong, A. Walsh, and S.-H. Wei, Appl. Phys. Lett. **94**, 041903 (2009).
[10] J. Paier, R. Asahi, A. Nagoya, and G. Kresse, Phys. Rev. B **79**, 115126 (2009).

[11]K. Ramasamy, M. A. Malik, and P. O'Brien, Chem. Commun. **48**, 5703 (2012).
[12]W. M. Hlaing Oo, J. L. Johnson, A. Bhatia, E. A. Lund, M. M. Nowell, and M. A. Scarpulla, J. Electron. Mater. **40**, 2214 (2011).
[13]S. Chen, J.-H. Yang, X. G. Gong, A. Walsh, and S.-H. Wei, Phys. Rev. B **81**, 245204 (2010).
[14]A. Nagoya, R. Asahi, R. Wahl, and G. Kresse, Phys. Rev. B **81**, 113202 (2010).
[15]T. Maeda, S. Nakamura, and T. Wada, Jpn. J. Appl. Phys., Part 1 **50**, 04DP07 (2011).
[16]S. Chen, X. G. Gong, A. Walsh, and S.-H. Wei, Appl. Phys. Lett. **96**, 021902 (2010).
[17]R. Scheer and H.-W. Schock, *Chalcogenide Photovoltaics: Physics, Technologies, and Thin Film Devices* (Wiley-VCH, Verlag & Co., Weinheim, 2011), p. 368.
[18]K. L. Chopra and S. R. Das, *Thin Films Solar Cells* (Plenum Press, New York, 1983), p. 607.
[19]F. A. Kreger, *The Chemistry of Imperfect Crystal* (North-Holland Publishing Company, 1974), p. 988.
[20]D. T. J. Hurle, J. Appl. Phys. **107**, 121301 (2010).
[21]O. Porat and I. Riess, Solid State Ionics **81**, 29 (1995).
[22]M. A. Berding, M. van Schilfgaarde, and A. Sher, Phys. Rev. B **50**, 1519 (1994).
[23]R. Grill and A. Zappettini, Prog. Cryst. Growth Charact. Mater. **48/49**, 209 (2004).
[24]M. A. Berding, Phys. Rev. B **60**, 8943 (1999).
[25]E. G. Seebauer and M. C. Kratzer, *Charged Semiconductor Defects* (Springer, Lexington, 2011), p. 294.
[26]A. Alkauskas, P. Deak, J. Neugebauer, A. Pasquarello, and C. G. Van de Walle, *Advanced Calculations for Defects in Materials* (Wiley-VCH Verlag, Weinheim, 2011), p. 384.
[27]S. B. Zhang, S.-H. Wei, and A. Zunger, Phys. Rev. B **57**, 9642 (1998).
[28]S.-H. Wei and S. B. Zhang J. Phys. Chem. Solids **66**, 1994 (2005).
[29]C. G. Van de Walle and J. Neugebauer, J. Appl. Phys. **95**, 3851 (2004).
[30]A. Kuwabara, Sci. Technol. Adv. Mater. **8**, 519 (2007).
[31]V. Kosyak, A. Opanasyuk, and I. Protsenko, Radiat. Meas. **42**, 855 (2007).
[32]V. Kosyak, M. Kolesnyk, and A. Opanasyuk, J. Mater. Sci. **V19**, S375 (2008).
[33]D. Kurbatov, V. Kosyak, and A. Opanasyuk, Physica B **4004**, 502 (2009).
[34]S. Siebentritt and U. Rau, *Wide-Gap Chalcopyrites* (Springer, Heidelberg, 2006), p. 257.
[35]S. Siebentritt, M. Igalson, C. Persson, and S. Lany, Prog. Photovoltaics **18**, 390 (2010).
[36]I.-H. Choi, C.-H. Choi, and J.-W. Lee, Phys. Status Solidi A **209**, 1192 (2012).
[37]T. Maeda and T. Wada, J. Phys. Chem. Solids **66**, 1924 (2005).
[38]S.-H. Wei, S. B. Zhang, and A. Zunger, Appl. Phys. Lett. **72**, 3199 (1998).
[39]S. Lany and A. Zunger, J. Appl. Phys. **100**, 113725 (2006).
[40]A. Zunger, Thin Solid Films **515**, 6160 (2007).
[41]H. J. Von Bardelben, Sol. Cells **16**, 381 (1986).
[42]T. J. Anderson and B. J. Stanbery, National Renewable Energy Laboratory Report No. NREL/SR-520-30391, 1998.
[43]T. Gurel, C. Sevik, and T. Cagın, Phys. Rev. B **84**, 205201 (2011).
[44]N. B. Mortazavi Amiri and A. Postnikov, Phys. Rev. B **82**, 205204 (2010).
[45]M. J. Romero, H. Du, G. Teeter, Y. Yan, and M. M. Al-Jassim, Phys. Rev. B **84**, 165324 (2011).
[46]J. P. Leitao, N. M. Santos, P. A. Fernandes, and P. M. P. Salome, Phys. Rev. B **84**, 024120 (2011).
[47]V. Kosyak, M. A. Karmarkar, and M. A. Scarpulla, Appl. Phys. Lett. **100**, 263903 (2012).
[48]I. D. Olekseyuk, I. V. Dudchak, and L. V. Piskach, J. Alloys Compd. **368**, 135 (2004).
[49]L. A. Girifalco, *Statistical Physics of Materials* (Wiley-VCH Verlag, Weinheim, 1973), p. 346.
[50]R. Steudel, *Elemental Sulfur and Sulfur-Rich Compounds I* (Springer, Berlin, 2003), p. 202.
[51]F. Schwabl, *Statistical Mechanics* (Springer-Verlag, Berlin, 2002), p. 573.
[52]D. A. McQuarrie, *Statistical Mechanics* (University Science Books, Sausalito, 2000), p. 643.
[53]See http://www.icmab.es/siesta/ for SIESTA homepage.
[54]P. Ordejón, E. Artacho, and J. M. Soler, Phys. Rev. B **53**, R10441 (1996).
[55]J. M. Soler, E. Artacho, J. D. Gale, A. García, J. Junquera, P. Ordejón, and D. Sánchez-Portal, J. Phys.: Condens. Matter **14**, 2745 (2002).
[56]D. C. Look, *Electrical Characterization of GaAs Materials and Devices* (Wiley, New York, 1989), p. 280.
[57]C. Persson, J. Appl. Phys. **107**, 053710 (2010).
[58]M. Grundmann, *The Physics of Semiconductors* (Springer, Berlin, 2010), p. 863.
[59]J. S. Blakemore, *Semiconductor Statistics* (Dover, Mineola, 1987), p. 381.
[60]B. Mayer, Chem. Rev. **76**, 382 (1976).